Eur. Phys. J. Special Topics **225**, 335–341 (2016)

DOI: 10.1140/epjst/e2016-02634-7

THE EUROPEAN PHYSICAL JOURNAL SPECIAL TOPICS

Regular Article

Shock compression of [001] single crystal silicon

S. Zhao[1], E.N. Hahn[1], B. Kad[1], B.A. Remington[2], and E.M. Bringa[3,4], and M.A. Meyers[1,a]

[1] University of California San Diego, La Jolla, CA 92093, USA
[2] Lawrence Livermore National Laboratory, Livermore, CA 94550, USA
[3] Universidad Nacional de Cuyo, Mendoza 5500, Argentina
[4] CONICET, Mendoza 5500, Argentina

Received 25 August 2015 / Received in final form 10 February 2016
Published online 14 March 2016

Abstract. Silicon is ubiquitous in our advanced technological society, yet our current understanding of change to its mechanical response at extreme pressures and strain-rates is far from complete. This is due to its brittleness, making recovery experiments difficult. High-power, short-duration, laser-driven, shock compression and recovery experiments on [001] silicon (using impedance-matched momentum traps) unveiled remarkable structural changes observed by transmission electron microscopy. As laser energy increases, corresponding to an increase in peak shock pressure, the following plastic responses are are observed: surface cleavage along {111} planes, dislocations and stacking faults; bands of amorphized material initially forming on crystallographic orientations consistent with dislocation slip; and coarse regions of amorphized material. Molecular dynamics simulations approach equivalent length and time scales to laser experiments and reveal the evolution of shock-induced partial dislocations and their crucial role in the preliminary stages of amorphization. Application of coupled hydrostatic and shear stresses produce amorphization below the hydrostatically determined critical melting pressure under dynamic shock compression.

1 Introduction

The shock response of silicon was reported as early as 1960s [1]. Various experimental investigations were carried out, with focuses on shock Hugoniot data [2], high pressure phase transformation [3], and inhomogeneous plastic flow [4], among many others [5–13]. More recently, the shock behavior of silicon has also been studied computationally [14]. Taken together, these reports sometimes present contradictory results. Loveridge-Smith et al. [2] reported an anomalous elastic limit of silicon under laser shock compression whereas Smith et al. [4] reported heterogeneous plastic flow under similar experiment conditions. Molecular dynamics (MD) simulations suggest that silicon undergoes a phase transition when subjected to shock compression [14].

[a] e-mail: mameyers@eng.ucsd.edu

The justification and conflation of these results require both post-shock microstructural characterization as well as the development/selection of appropriate interatomic potentials. However, observations of the microstructural mechanisms of shock-loaded silicon are rarely seen in the literature due to the difficulty of sample recovery. Recently, we developed a new methodology to recover silicon single crystals from high-pressure laser shock compression experiments [15]. Direct microstructural evidence allows for an assessment of interatomic potential transferability to account for dynamic high pressure and strain-rate environments.

2 Experimental and computational methodology

2.1 Laser shock compression experiment

A high-power short-pulsed laser was used to conduct shock compression experiments on [001]-oriented silicon monocrystals. Experiments were conducted using the laser source located at the Omega Laser Facility, Laboratory for Laser Energetics, University of Rochester. The experimental set-up is illustrated schematically in Fig. 1. Before laser shock, silicon targets were encapsulated in an aluminum cup by heating the capsule and allowing it to cool, thereby confining the Si monocrystal.

2.2 Microstructure characterization

The post-shock microstructure was characterized by optical microscopy (OM), scanning electron microscopy (SEM) and transmission electron microscopy (TEM). Focused ion beam (FIB) is used to cut the TEM samples directly from the centers of the shock surface at prescribed orientations.

2.3 Molecular dynamic simulation

Silicon is among the most common computationally studied systems and a wide variety of semi-empirical potentials span numerous environments that place explicit emphasis on fitting to specific properties. Here we are concerned with the plastic response of silicon at elevated pressures and associated temperatures. Potentially applicable interatomic potentials include Stillinger-Weber [16] addressing dislocation properties, and Tersoff derived potentials placing emphasis largely on phase transitions [17]. More recent iterations of the Tersoff-type bond order potential include fitting to thermal properties, point defect energies, and Si-C interactions [18]. MOD, developed by Kumagai [19], is one such Tersoff family potential that simultaneously fit melting point, elastic constants, and multiple structural energies. MOD has since been shown to produce accurate kinetics of the crystalline to liquid transition [20] as well as a confirmed decrease in melting temperature with compression to 3 GPa [21] following the expected negative Clausius-Clapeyron slope trend. A previous study indicated that MOD produces acceptable general stacking-fault energies in addition to many pressure dependent properties up to 25 GPa [15]. Due to the negative Clasius-Clapeyron slope and strongly anticipated temperature rise in both simulated impact and around the laser ablated regime, it is critical that the chosen potential be able to accurately reflect the role of temperature-dependent plasticity and phase change. For this reason, we expect the MOD potential to be most applicable to our simulations of high pressure and temperature. Molecular Dynamics simulations were accomplished through the LAMMPS package [22] and atomic visualization through OVITO [23].

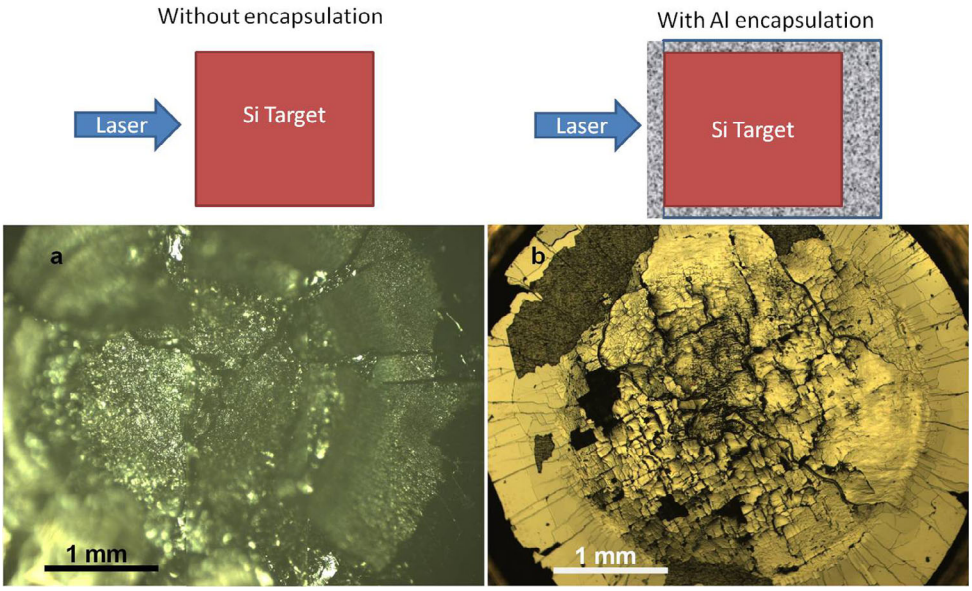

Fig. 1. Schematic drawing of the target assembly and the corresponding optical microscopy images: a) naked target without any protection: the sample shattered and the surface roughness caused the difficulties in focusing; b) target with aluminum encapsulation: the sample was recovered successfully with crack pattern on the surface, enabling the subsequent TEM analysis. Both targets were shocked by a high amplitude pulsed blue laser (λ=351 nm) with a similar peak energy (E = 100 J).

Simulated shock experiments were conducted by impacting a frozen piston traveling at a desired particle velocity with a multi-million atom silicon crystal of [001] orientation aligned with the shock direction. This method is a slight adjustment of the linearly ramped frozen piston shock method implemented by Bringa [24]. Initial separation between the piston and sample allows for dimerization of the (001) surface, a type of reconstruction that lowers surface energy and produces a non-zero defect density more representative of the physical reality of the system.

3 Results and discussions

Figure 1 shows the optical micrographs of the as-shocked surface of silicon at a similar laser energy level of 100 J, (a) without aluminum capsule and (b) with Al encapsulation. It is clearly evidenced that surface damage is dramatically diminished when the Al protective encapsulation is used. The sample without protection shattered into pieces, leaving a rough surface morphology whereas the encapsulated target was recovered successfully. Aluminum was chosen as an encapsulation medium due to its machinability and, more importantly, similar acoustic impedance (Z = density multiplied by the sound velocity) to silicon; Z_{Al} = 17.33 and Z_{Si} = 19.7 MPa · s/m, respectively. By matching acoustic impedance, reflected tensile shock waves are minimized while transmitted shock waves are maximized. Through this methodology, normally brittle silicon was able to be recovered without excessive tensile cracking.

Numerous micro-cracks were observed on the shock surface, and the network crack pattern clearly shows preferential crystallographic orientation. It is accepted that {111} planes are the easiest cleavage plane in silicon, therefore the crack lines are

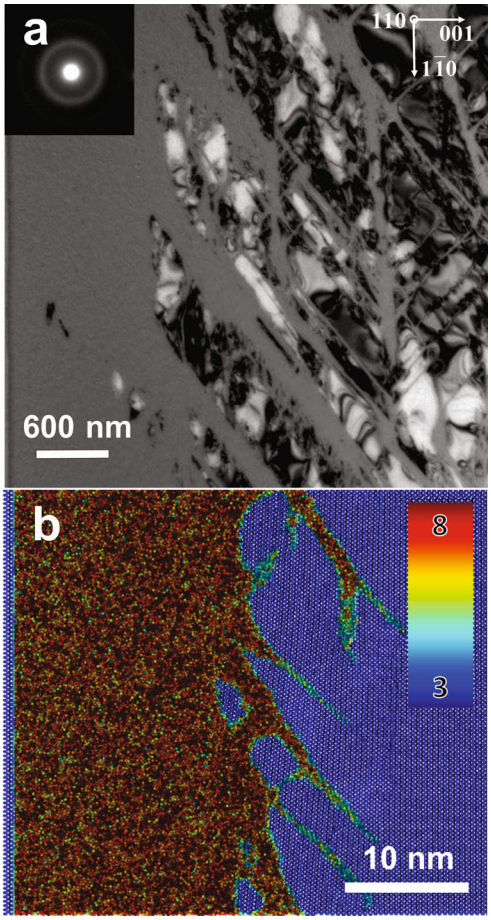

Fig. 2. TEM micrograph (a) of the amorphous materials observed in the 100 J laser shocked silicon target; and MD simulation (b) with a roughly equivalent peak shock pressure shows a similar feature in a, the color scale in b represent for coordination number.

their traces on (001) shock surface, i.e. either $[1\bar{1}0]$ or [110], which are perpendicular to each other.

Figure 2 illustrates the shock-induced amorphization of silicon. TEM images shows that the amorphous region has a thick layer on the surface, while multiple bands penetrate inwards the crystals. The bands clearly show some crystallographic characteristics, i.e. they reasonably align with the {111} slip plane (of dislocations) in silicon. Molecular dynamics simulations also predict amorphization and show similar layer and band features. MD simulation also indicates that many of these bands propagate in {111} planes as expected, but there is also evidence of {110} bands. Both Stillinger-Weber and MOD potentials have been shown to predict the quasi-stability of the {110} stacking faults under compression, but little experimental post shock evidence is expected to remain due to some extent of unavoidable rarefaction waves [15,25].

Furthermore, molecular dynamics shows that indeed the shear stress prior to plastic deformation is significant and can be as much as half the pressure depending on compression. After defect nucleation, the shear stress begins to relax and then drops to zero within the amorphous region. Full relaxation of shear stress does not confirm

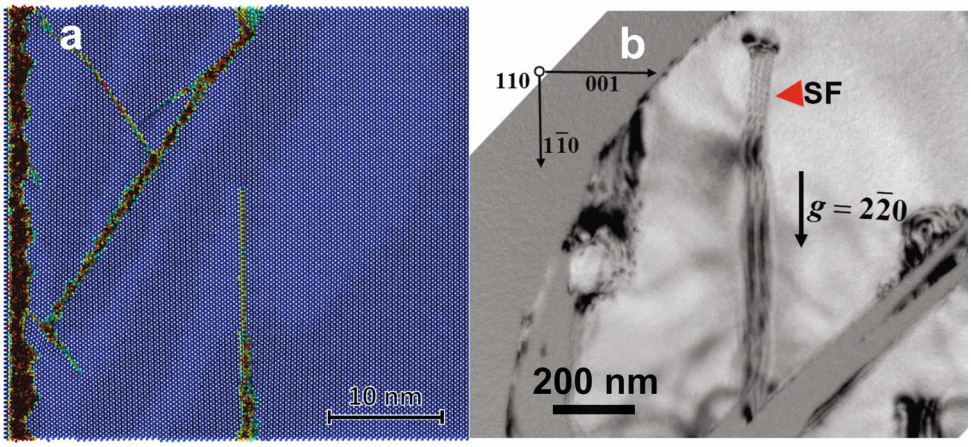

Fig. 3. MD simulation (a) shows several 111 stacking fault as the precursor of the amorphization; and TEM observation (b) also shows stacking faults bounding the amorphous materials.

or deny this as a solid state process. A melt would be unable to sustain shear stress, but full 3D relaxation during amorphization is just as plausible. Silicon is known to have at least two amorphous phases, one high density and one low density, in addition to the disordered liquid phase.

MD simulation, as shown in Fig. 3, indicates that numerous stacking faults were generated before amorphization. These stacking fault are mostly of 111 and 110 type. The TEM image in the upper-right inset also shows that stacking faults bounds the edge of an amorphous band.

A tridimensional view of the MD simulated microstructure of shocked silicon is presented in Fig. 4 with marks indicating multiple stacking-fault variants. Such interaction of these stacking faults is expected to occur under experimental laser shock compression, leading to large defect densities and defect localization effects such as loss of atomic order and plastic heating.

Silicon is a material with negative Clapeyron slope; it melts with an increased volume and thus the melting temperature decreases with elevating pressure. Therefore, it is possible to melt silicon by pressure at a temperature much lower than the ambient melting temperature. In light of this, Deb et al. [26] reported that when pressurizing silicon in a diamond anvil cell at room temperature, it will undergo amorphization at a pressure of 15 GPa. Shear stress plays a very important yet often neglected role in structural transformation of materials [5,6,27–30]. When shock waves are launched in a solid material, a uniaxial strain state is established [31], with both high hydrostatic (pressure) and deviatoric (shear) stress components. It is suggested that the high shear stress, coupled with the pressure associated leads to the amorphization, i.e., the existence of high shear stress lower the threshold of the pressure induced amorphization of silicon. Unlike pressure, shear stress will induce the generation of lattice defects such as dislocations, stacking faults, and twinning. The motion of these defects increases the local disorder of the lattice and may be associated with significant heating. Under quasi-static loading, the heat can be dissipated quickly to the surrounding materials without causing a temperature rise. However, under shock loading, an adiabatic condition is established in the sheared region and the temperature will rise correspondingly. If the temperatures reaches the diminished melting point of the material, melting will occur. Furthermore, the rapid release of the stress pulse causes a self-quenching mechanism; if the cooling rate is sufficiently high it will lead to the

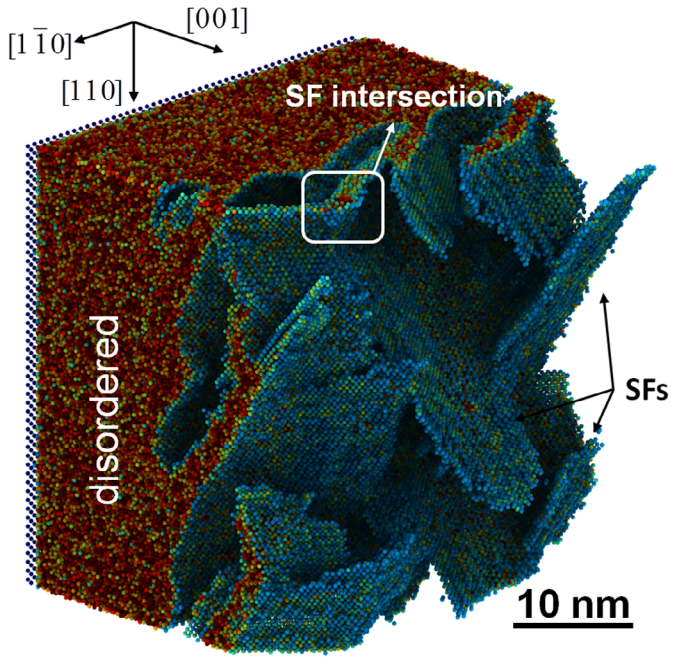

Fig. 4. Tridimensional view of the stacking faults (SF) as the precursors of the amorphization: multiple stacking faults and their intersections can be observed ahead of the disordered region. A disordered region was left behind.

preservation of the disordered structure and amorphous materials can be produced. Moreover, the co-existing pressure will lower the melting point of the silicon, which, in turn, facilitates the amorphization.

4 Conclusions

In this investigation, the post-laser shock microstructure of [001] silicon single crystal was characterized by OM, SEM and TEM. Despite a semi-brittle failure quantified by the crack network seen on the shocked surface, it is shown that, beyond certain laser energy threshold, silicon undergoes amorphization. Laser-induced transformation creates a thick amorphous layer adjacent to the shock surface and amorphous bands of varying thickness that penetrate into the sample. Both large-scale molecular dynamics simulation and TEM observation indicate that shock-induced stacking faults play an important role in this process. It is therefore proposed that the high magnitude of the shear stresses, in coordination with pressure, leads to the formation of the amorphous silicon under shock conditions. This finding may ultimately provide a new methodology to fabricate bulk amorphous silicon of particular interest to the semiconductor industry.

References

1. L.V. Al'tshuler, Sov Phys. Uspekhi **8**, 52 (1965)
2. A. Loveridge-Smith, A. Allen, J. Belak, T. Boehly, A. Hauer, B. Holian, D. Kalantar, G. Kyrala, R.W. Lee, P. Lomdahl, M.A. Meyers, D. Paisley, S. Pollaine, B. Remington, D.C. Swift, S. Weber, J.S. Wark, Phys. Rev. Lett. **86**, 2349 (2010)

3. H. Kishimura, H. Matsumoto, J. Appl. Phys. **103**, 023505 (2008)
4. R.F. Smith, C.A. Bolme, D.J. Erskine, P.M. Celliers, S. Ali, J.H. Eggert, S.L. Brygoo, B.D. Hammel, J. Wang, G.W. Collins, J. Appl. Phys. **114**, 133504 (2013)
5. N.S. Enikolopyan, A.A. Zharov, V.A. Zhorin, A.G. Kazakevich, P.A. Yampolski, J. Appl. Mech. Tech. Phys. **15**, 116 (1974)
6. S.M. Walley, J.E. Balzer, W.G. Pround, J.E. Field, Proc. R. Soc. Lond. A. **456**, 1483 (2000)
7. M.N. Pavlovskii, Sov. Phys. Solid State. **9**, 2514 (1967)
8. W.H. Gust, E.B. Royce, J. Appl. Phys. **42**, 1897 (1971)
9. T. Goto, T. Sato, Y. Syono, Jpn J. Appl. Phys. Lett. **21**, 369 (1982)
10. J.S. Wark, R.R. Whitlock, A. Haner, J.E. Swain, P.J. Solone, Phys. Rev. B. **35**, 9391 (1987)
11. J. Ren, S.S. Orlov, L. Hesselink, J. Appl. Phys. **97**, 104304 (2005)
12. G.J. Cheng, M.A. Shehadeh, Int. J. Plast. **22**, 2171 (2006)
13. G.J. Cheng, M.A. Shehadeh, Scr. Mater. **53**, 1013 (2005)
14. G. Mogni, A. Higginbotham, K. Gaál-Nagy, N. Park, J.S. Wark, Phys. Rev. B. **89**, 064104 (2014)
15. S. Zhao, B. Kad, E.N. Hahn, B.A. Remington, C.E. Wehrenburg, C.M. Huntington, H.S. Park, E.M. Bringa, K. More, M.A. Meyers, Extreme Mech. Lett. **5**, 74 (2015)
16. F.H. Stillinger, T.A. Weber, Phys. Rev. B. **31**, 5262 (1985)
17. J. Tersoff, Phys. Rev. B., **38** 9902
18. P. Erhart, K. Albe, Phys. Rev. B. **71**, 035211 (2005)
19. T. Kumagai, S. Izumi, S. Hara, S. Sakai, Comput. Mater. Sci. **39**, 457 (2007)
20. P.K. Schelling, Comput. Mater. Sci. **44**, 274 (2008)
21. V.S. Dozhdikov, A.Y. Basharin, P.R. Levashov, J. Chem. Phys. **137**, 054502 (2012)
22. S. Plimpton, J. Comput. Phys. **117**, 1 (1995)
23. A. Stukowski, Model. Simul. Mater. Sci. Eng. **18**, 015012 (2010)
24. E.M. Bringa, K. Rosolankova, R.E. Rudd, B.A. Remington, J.S. Wark, M. Duchaineau, Nat. Mater. **5**, 805
25. L.M. Hale, D.B. Zhang, X. Zhou, J.A. Zimmerman, N.R. Moody, T. Dumitrica, R. Ballarini, W.W. Gerberich **54**, 280 (2012)
26. S.K. Deb, M. Wilding, M. Somayazulu, P.F. McMillan, Nature **414**, 528 (2001)
27. P.W. Bridgman, Phys. Rev. **48**, 825 (1935)
28. H.C. Chen, J.C. Lasalvia, V.F. Nesterenko, M.A. Meyers, Acta Mater. **46**, 3033 (1998)
29. E. Teller, J. Chem. Phys. **36**, 901 (1962)
30. G. Duvall, R. Graham, Rev. Mod. Phys. **49**, 523 (1977)
31. M.A. Meyers, Dyn. Behav. Mater. (John Wiley & Sons, 1994)